Budding and Fission of a multiphase vesicle

Jean-Marc Allain, Martine Ben Amar

Budding and Fission of a multiphase vesicle

Jean-Marc ALLAIN and Martine BEN AMAR

Laboratoire de Physique Statistique, CNRS-UMR 8550,

Ecole Normale Supérieure, 24, rue Lhomond 75231 Paris France

April 8, 2005

Abstract

We present a model of bi-phasic vesicle in the limit of large surface tension. In this regime, the vesicle is completely stretched and well described by two spherical caps with a fold which concentrates the membrane stress. The conservation laws and geometric constraints restrict the space of possible shapes to a pair of solutions labeled by a parameter τ given by *line tension/pressure*. For a given τ value, the two solutions differ by the length of the interface between domains. For a critical value τ_c, the two vesicle shapes become identical and no solution exists above this critical value. This model sheds new light on two proposed mechanisms (osmotic shocks and molecule absorption) to explain the budding and the fission in recent experiments.

1 Introduction

The cell membrane is a bilayer made out of a mixture of lipid species. The membrane is both the boundary of the cell and an interface inside the cell, separating different compartments. This soft structure is responsible for many biological properties. Intracellular traffic is also realized by membrane structures: a membrane vesicle buds from one compartment, travels through the cytosol and fuses with another compartment. Despite the fluidity of the lipid bilayer, the cellular membrane presents a lateral inhomogeneity due the formation of dynamical microdomains, called rafts (Simons and Ikonen, 1997). These microdomains have been shown to be rich in cholesterol and sphingolipid (Brown and London, 2000). *In vivo*, the rafts have not been directly observed but their size has been estimated to be between 20 and 700 nm (Chazal and Gerlier, 2003). A central question in membrane biology and biophysics is to understand how this spatial organization is used by the cell, in particular to favor interactions with proteins. Due to their size and specific composition, it has been argued that rafts play a role in protein docking, signaling, intracellular traffic (van Meer and Sprong, 2004) or virus budding (Chazal and Gerlier, 2003).

Recently, a model system of Giant Unilammelar Vesicles (GUV) including sphingomyelin-cholesterol domains was developed (Dietrich et al., 2001). These domains, which are supposed to reproduce raft composition, are the result of a phase separation of the lipid species (Veatch and Keller, 2003). They are more structured than the surrounding classical liquid bilayer but remain in a liquid state. For this reason, they are called "liquid-ordered" domains whereas the classical membrane is called "liquid-disordered". A large num-

ber of studies have focused on the thermodynamic of liquid-ordered phases, in particular the effect of temperature or composition changes on domain formation (de Almeida et al., 2003; Veatch and Keller, 2003). Multi-phase vesicles are elegant and efficient tools to study the mechanical properties of microdomains. It can be used to understand how rafts bud and make daughter vesicles for intracellular traffic, but also how detergent addition can isolate rafts from the cell membrane. Recent experiments have shown that liquid-ordered domains can be separated from the initial vesicle by using tubular deformations (Allain et al., 2004), osmotic shocks (Baumgart et al., 2003; Bassereau and Roux, personnal communication) or absorption of external molecules like proteins or detergents (Staneva et al., 2004; Staneva et al., submitted). Here, we develop a macroscopic theory for the two last situations. Our model describes the budding preceeding the fission where the liquid-ordered domain is lift up from the liquid-disordered vesicle.

Budding and fission have already attracted many theoretical works for homogeneous (Jaric et al., 1995; Seifert, 1997; Dbereiner et al., 1997; Tanaka et al., 2004; Sens, 2004) or inhomogeneous (Seifert, 1993; Jlicher and Lipowsky, 1996; Kohyama et al., 2003; Laradji and Sunil Kumar, 2004; Harden et al., submitted) membranes. The models vary depending on the physical interactions involved but they are all based on the minimization of the bilayer energy (Helfrich, 1973). Due to the non-linearity of the steady-shape equations, a numerical treatment is often required. We focus our attention on multi-phase vesicles slightly stretched, a situation often encountered in experiments. In this case, osmotic pressure effects dominate and we show that the vesicle can be described by two spherical caps with an elastic junction. The variational

3

procedure with surface constraints allows to find two solutions for any ratio $\tau = line\ tension/pressure$ less than a critical value τ_c. The stable solution is the one observed experimentally. An osmotic shock increases the control parameter τ and so destabilizes the stable solution which may lead the system to a complete fission of the neck. The case of detergents is slightly different since it requires an energy model for molecular absorption in the membrane. When detergent molecules are added in the membrane, they locally deform the bilayer. According to Leibler's model (Leibler, 1986), these curvature defects can be taken into account by a term in the energy proportional to both the average curvature and the concentration of molecules. Homogeneous concentration of molecules is favored away from the interface between domains. At the junction, a concentration gradient appears. If the chemical inhomogeneity is localized at the junction, the addition of molecules leads to an increase of the effective line tension inducing a budding and a possible separation into two independent vesicles.

Our model explains qualitatively and even quantitatively the budding and fission created by osmotic shocks or proteins absorption. It is a physical approach based on continuum description and its domain of validity ends at the molecular level. Because of its simplicity, extension and application to other processes may be achieved easily.

2   Membrane description.

2.1   Inhomogeneous lipid bilayer.

We consider an inhomogeneous vesicle constituted by two lipid phases: a 'liquid-ordered' (l_o) and a 'liquid-disordered' (l_d). Both phases are in the liquid state but the (l_o) domain is more structured than the (l_d) phase due to the following reasons: there are specific interactions between molecules (Li et al., 2001) and/or there is an optimization of biphilic space packing (Holopainen et al., 2004). Steady morphologies and their out-of-plane deformations are well described by the Canham and Helfrich's model with energy for each phase i given by:

$$F_m^i = \int\limits_S \left[2\kappa_i \mathsf{H}^2 + \kappa_G^{(i)} \mathsf{K} + \Sigma_i \right] dS \qquad (1)$$

H and K are respectively the mean and Gaussian curvature. The elastic bending rigidity κ_i and Gaussian rigidity $\kappa_G^{(i)}$ are expected to be higher in the l_o phase. Typical values can be found for example in (Lipowsky and Sackmann, 1995): $\kappa_{l_d} \simeq 20 \mathrm{k_b T}$ and $\kappa_{l_o} \simeq 80 \mathrm{k_b T}$. Values of Gaussian moduli are notoriously more difficult to measure but a recent study mentions values of order $\kappa_G^{(i)} = -0.83\kappa_i$ (Siegel and Kozlov, 2004). Although F_m^i is a surface integral, the Gaussian contribution to the energy is indeed a contour integral calculated at the interface between the two domains, due to the Gauss-Bonnet theorem.

The last contribution in Eq.1 is related to the possible extension of the membrane. In the case of a stretched vesicle, this contribution is large compared to the elastic energy and the membrane surface can be considered as constant. This is taken into account by introducing the Lagrange multiplier

Σ_i.

The total energy of the two-domain vesicle includes the energy (1) of each phase plus two coupling terms. First, a sharp interface of vanishing thickness exists between the l_o and l_d phases. Any increase of its length requires an energy proportional to a line tension σ. Second, the vesicle membrane is lightly permeable to the water but not to the ions or big molecules present in the surrounding water medium. This induces an osmotic pressure P. The energy of the coupling terms is:

$$F_c = \sigma \int_C dl - P \int dV \qquad (2)$$

2.2 Proteins or detergent-membrane interactions

External molecules such as proteins or detergents can be absorbed in both phases but with different efficiencies. Their introduction in the membrane is well described by a Landau's approach with an optimal homogeneous concentration ϕ_{eq}. Departure from this value or inhomogeneity of concentration ϕ has a cost in energy, assumed quadratic to leading order. The energy cost is given by two positive constants in each phase: α_i and β_i. If the proteins are soluble or not in the surrounding medium, we can either set the number of these molecules in each phase or set the chemical potential μ_i of the phase i. We choose to fix μ_i but this has no real incidence on the results since it only affects the definition of μ_i. Therefore the free chemical energy of absorption for each phase is:

$$F_p^i = \int_{S_i} \left(\frac{\alpha_i}{2}(\phi - \phi_{eq_i})^2 + \frac{\beta_i}{2}(\nabla\phi)^2 + \mu_i\phi \right) dS + \int_{S_i} \Lambda_i \mathsf{H}\phi dS \qquad (3)$$

6

The last integral in Eq.3 represents the local distortion of the membrane induced by the absorbed molecules (Leibler, 1986; Bickel et al., 2001). It is proportional to the mean curvature of the membrane with a weight depending on the local concentration ϕ, as suggested by S. Leibler (Leibler, 1986), Λ_i being a coupling constant. The absorption process itself affects differently the two leaflets of the vesicle. We restrict our attention to the case where the adsorption takes place on one side only. In such case, Λ_i is positive on the outer side absorption and negative on the inner side. When the two layers are affected by absorption, two concentration fields are necessary and our theoretical framework can be easily adapted to address such situation. Taken into account all previous contributions, the total free energy for the system is given by:

$$F_{TOT} = F_m^o + F_m^d + F_p^o + F_p^d + F_c \qquad (4)$$

The usual variation procedure to identify extrema of this energy produces the so called Euler-Lagrange equations.

2.3   Euler-Lagrange equations.

Minimization of the free energy F_{TOT} gives the static solutions for the membrane. Looking for axisymmetric shapes, we choose the cylindrical coordinates and we parameterize the surface by the arc-length s. The vesicle shape is given by $r(s)$ and $\psi(s)$ (see Fig. 1). We have derived the Euler-Lagrange

equations associated with F_{TOT} (Allain and Ben Amar, 2004). They are

$$\psi'' = \frac{\sin(\psi)\cos(\psi)}{r^2} - \frac{\psi'}{r}\cos(\psi) - \frac{Pr}{2\kappa_i}\cos(\psi) + \frac{\gamma}{\kappa_i r}\sin(\psi) + \frac{\Lambda_i}{\kappa_i}\phi' \quad (5a)$$

$$\gamma' = \frac{\kappa_i}{2}\psi'^2 - \frac{\kappa}{2r^2}\sin(\psi)^2 + \tilde{\Sigma}_i - Pr\sin(\psi) - \Lambda_i\phi\psi' + \frac{\alpha_i}{2}\phi^2 \quad (5b)$$

$$+ \frac{\beta_i}{2}\phi'^2 + \tilde{\mu}_i\phi$$

$$\phi'' = -\phi'\frac{\cos(\psi)}{r} - \frac{\Lambda_i}{\beta_i}\left(\frac{\sin(\psi)}{r} + \psi'\right) + \frac{\alpha_i}{\beta_i}\phi + \frac{\tilde{\mu}_i}{\beta_i} \quad (5c)$$

$$r' = \cos(\psi). \quad (5d)$$

These equations have to be solved with the suitable boundary conditions at the border between the two domains. To simplify the notations, we introduce the following parameters: $\tilde{\Sigma}_i = \Sigma_i + \alpha_i/2\phi_{eq_i}^2$ and $\tilde{\mu}_i = \mu_i - \alpha_i\phi_{eq_i}$. Assuming continuity of both the radius r, the angle ψ and the molecules concentration ϕ, the variational procedure gives also three equations for the boundary conditions:

$$\kappa_1\psi'(s_J - \epsilon)r(s_J) + (\kappa_1 + \kappa_{G_1})\sin(\psi(s_J)) - \Lambda_1\phi(s_J)r(s_J) \quad (6a)$$

$$-\kappa_2\psi'(s_J + \epsilon)r(s_J) - (\kappa_2 + \kappa_{G_2})\sin(\psi(s_J)) + \Lambda_2\phi(s_J)r(s_J) = 0,$$

$$\gamma(s_J - \epsilon) - \gamma(s_J + \epsilon) + \sigma = 0 \quad (6b)$$

$$\beta_1\phi'(s_J - \epsilon) - \beta_2\phi'(s_J + \epsilon) = 0. \quad (6c)$$

where s_J is the arc-length at the junction, label 1 denotes the phase for $s \leq s_J$ and label 2 the phase for $s \geq s_J$.

Since these equations are highly non-linear, there is no exact solutions for arbitrary values of the physical parameters. However further analytical progress can be obtained in the limit of large pressure (stretched membrane). Remarkably, this treatment only requires simple analytical algebra and allows to explain experimental features such as the complete budding of the ordered

8

phase obtained by different groups using either osmotic shocks (Baumgart et al., 2003), proteins (Staneva et al., 2004) or detergent molecules (Staneva et al., submitted)

3 Analytical treatment of the membrane shape.

We first consider a membrane without absorbed molecules. A solution of the Euler-Lagrange equations can be easily found if we discard the contribution from the elasticity. We use this simple solution as zeroth order and correct it for small but not vanishing values of the bending rigidity by using boundary layer analysis. We consider also the inclusion of molecules with no chemical activity. They are described in the model by curvature defects. For a weak coupling between curvature and concentration, a similar strategy is used to understand how the molecules affect the membrane shape.

3.1 The exact zero-order model: the capillary solution.

For stretched membrane without absorbed molecules ($\phi = 0$), it is believed that after electro-formation of GUV vesicles the osmotic pressure dominates the elastic energy. When $\kappa_i = 0$ in both phases, a solution of the Euler-Lagrange equation is made of two spherical caps defined by a set of four geometrical parameters: the radii of the two caps R_1, R_2 and the two angles at the boundary θ_1 and θ_2 (see Fig. 2). The contact between the two caps gives a first continuity relation

$$R_1 \sin \theta_1 = R_2 \sin \theta_2. \tag{7}$$

The Euler-Lagrange equations (Eq.5) give the values of the two Lagrange multipliers Σ_i and γ_i, without direct information on the vesicle shape:

$$2\Sigma_i = PR_i, \tag{8a}$$

$$\gamma_i(s) = \frac{PR_i^2}{2} \sin \psi \cos \psi. \tag{8b}$$

the angle ψ being proportional to the arc-length s. Only the boundary condition and the conservation of the area of each phase give the possibility to fix completely the ideal shape. From Eq.6, we deduce:

$$R_1^2 \sin \theta_1 \cos \theta_1 = R_2^2 \sin \theta_2 \cos \theta_2 - \frac{2\sigma}{P}. \tag{9}$$

The shape is controlled by the reduced line tension $\tau = \sigma/P$ (homogeneous to a surface), which can be adjusted by changing the osmotic pressure. As an example, from the figure (1b) in Baumgart et al.'s work (Baumgart et al., 2003), reproduced here in figure 4, we calculate $\tau = 20.5\mu m^2$, from estimated values of R_1, R_2, θ_1 and θ_2. Notice that in Baumgart's work, label 1 correspond to the l_d domain and label 2 to the l_o domain.

Solving Eq.7 and 9 for the above τ-value gives two possible solutions: $R_1 = 5.30\mu m$, $R_2 = 10.5\mu m$, $\theta_1 = 1.34$ and $\theta_2 = 0.514$, the measured values (Fig. 3(a)) but also $R_1 = 3.97\mu m$, $R_2 = 10.3\mu m$, $\theta_1 = 1.96$ and $\theta_2 = 0.364$ for the second solution (Fig. 3(b)). In order to explain why the first solution is preferred in the experiment, we calculate the energy which is restricted here to two contributions: $F_{TOT} = -PV + \sigma l$ with l the perimeter of the interface. Using a typical length scale $L_r = 10\mu m$, it is possible to construct the dimensionless energy $\tilde{F}_{TOT} = F_{TOT}/(\pi P L_r^3)$. Notice that the value of L_r does not affect the physics of the problem, it is used only to have

dimensionless lengths close to 1. So we obtain

$$\tilde{F}_{TOT} = -V/\pi L_r^3 + 2\tau R_1 \sin\theta_1/L_r^3, \tag{10}$$

which gives respectively (-1.380) compared to (-1.377), and shows that the experimental observed solution is stable while the other one is unstable as expected.

A systematic study of the pair of solutions for arbitrary values of τ is straightforward and the results are presented in figure 5. Figure 5a is a classical bifurcation diagram when a pair of solutions appears with opposite stability. In this problem, τ is the control parameter and the energy $\tilde{F}_{TOT}$ is the order parameter. These two solutions differ geometrically, the unstable solution presenting a smaller neck compared to the stable one (obvious if $\tau = 0$) (see Fig 5b). As τ increases, the two solutions become geometrically closer up to a finite value of $\tau_c = R_1 R_2/2$. Above the critical value ($\tau \geq \tau_c$), there is no connected solution of the Euler-Lagrange equations but the solution with two separated spheres remains.

This bifurcation diagram describing change in the topology of budding spheres is similar to the one found in the catenoid problem where a soap film is fixed on two parallel rings, separated by a small distance d compared to the radius of the ring. Two different minimal surfaces (with similar catenoid shapes) satisfy the variational equations derived from the capillary energy. The difference between these two shapes can be measured by the perimeter at mid-distance between the two rings. The catenoid with the smaller neck is unstable since its area is larger and, experimentally, the other catenoid is observed. However, as it is well known, as the distance d increases, the neck size decreases, the catenoid is destroyed and is replaced by two independent

11

disks (Ben Amar et al., 1998) with topology changes. This geometrical instability is not reversible. At the fission, the neck of the catenoid is not zero but the analytical calculation shows that the two catenoids, the stable and the unstable, have the same shape.

In our case, we are faced with the same type of capillary instability where there exist two similar solutions whose stabilities are governed by the energy. As the control parameter, here the effective line tension, is increased, the two solutions merge and a change of topology is expected at this point. We do not know if this change is irreversible since fission requires microscopic reorganization such as hemifission (Kozlovsky and Kozlov, 2003). Experimentally, the daughter vesicles can remain connected by a small filament of lipids but if the two vesicles move away, the process is of course not reversible. The critical value τ_c is determined by the fourth equation in Eq.9 which gives the equilibrium of the forces in the radial direction (axis r). The term in $\tau = \sigma/P$ is due to the line tension and its effect is to pinch the membrane. The two others terms (in R_1^2 and R_2^2) are related to the pressure force on the membrane and are bounded. The critical value τ_c is the value for the maximal force on the membrane. For higher line tension (or smaller pressure), it is no longer possible to compensate for the line tension which splits the system into two independent vesicles.

One important conclusion of this study is the fact that small domains are more easily ejected. This can be validated or invalidated experimentally when a vesicle has several l_o domains of various size. This conclusion is opposite to a floppy membrane whose shape is controlled by elasticity (Lipowsky and Dimova, 2003). To show this, we have varied the fraction f of the upper

12

domain (label 1) and we have calculated τ_c using the data of the experimental example (see Fig.6). Since the two phases are equivalent when elasticity is neglected, the results are the same for f and $1 - f$. The parameter τ_c increases with the size of the smallest domain. This result can be explained by a simple argument in the limiting case of a flat domain on a flat surface. If the radius of the domain is r, the pinching energy (due to the line tension) is approximatively σr and the resistance energy (due to the pressure) is approximatively Pr^3. The balance of the two energies gives $\sigma/P \approx r^2$. Therefore, it is harder to destabilize a large domain than a small one. Next, we study the robustness of the model when elasticity is taken into account.

3.2   The elasticity localization.

Comparing the bending energy (Eq.1) to the osmotic pressure energy (Eq.2) one finds that elastic effect can be neglected if $\kappa_i << PR_i^3$ in each phase. However, a discontinuity of the tangent appears at the interface between the two domains creating a singularity in the curvature. As soon as the bending modulus is exactly zero, this discontinuity produces an infinite elastic energy contribution, localized near the junction, in contradiction with the weakness of elasticity. We are faced with a classical boundary layer model, as found for example in the crumpling of an elastic plate (Ben Amar and Pomeau, 1997) or the folding of an elastic shell (Pogorelov, 1988). For small but not zero κ_i values, near the junction, the elastic effects smooth out the discontinuity by locally modifying the shape of the membrane (see Fig. 2) on a characteristic distance of order the elastic length l_e in each phase:

$$l_e = \sqrt{\frac{\kappa_i}{PR_i}}.$$

13

Using typical values for giant vesicles (Baumgart et al., 2003), we get $l_e \simeq 0.5\mu m$, which is very small compared to $R_i \simeq 10\mu m$. Therefore, we can model our system as two spherical caps slightly distorted at the junction on a distance of order l_e.

3.2.1 Fold description

Far away from the fold, the spherical solution (denoted by S) is a good approximation but not in the close vicinity of the fold better described by a boundary layer (denoted by B) of size $\tilde{l}_e = l_e/R_i$. We define a new arclength parameter $\tilde{l} = (\tilde{s} - \tilde{s}_J)/\tilde{l}_e$ and we decompose ψ, r and γ into

$$\psi = \psi_S + \psi_B(\tilde{l}) \quad ; \quad r = r_S + \tilde{l}_e r_B(\tilde{l}) \quad ; \quad \gamma = \gamma_S + \tilde{l}_e \gamma_B(\tilde{l}). \tag{11}$$

with $\psi_S = \theta_1$ or $\psi_S = \theta_2$. The quantities ψ_B, r_B and γ_B must vanish far away from the junction. Neglecting absorbed molecules, the leading order of Eq.5 gives

$$\ddot{\psi}_B = \sin \psi_B. \tag{12}$$

This is the pendulum equation with solution:

$$\tan(\psi_B/4) = \tan(\psi_{cusp}/4) \exp(\pm\tilde{l}). \tag{13}$$

The plus or minus sign is required for $\tilde{l}$ values, negative or positive: after the junction ($\tilde{s} \geq \tilde{s}_J$, $\tilde{l} \geq 0$), or before the junction ($\tilde{s} \leq \tilde{s}_J$, $\tilde{l} \leq 0$).

From Eq.4 and 12, we derive the elastic energy in each phase:

$$\frac{F_B}{2\pi P R_i^3} = \tilde{l}_e \sin \theta_i \left\{ 2 \left(1 - \cos \frac{\psi_{cusp} - \theta_i}{2} \right) \right. \tag{14}$$
$$\left. + \sin \theta_i \left[\sin \theta_i - \sin \left(\frac{\psi_{cusp} + \theta_i}{2} \right) \right] \right\}.$$

The elastic energy (Eq.14), localized at the junction is proportional to the interface length ($2\pi r_J = 2\pi \sin\theta_i$ in dimensionless parameters) and has the same effect as a line tension. Adding the two contributions, we obtain in physical units:

$$\sigma_{cusp} = \sqrt{\kappa_1 P R_1} \left\{ 2 \left[1 - \cos(\frac{\psi_{cusp} - \theta_1}{2}) \right] \right.$$
$$+ \sin\theta_1 \left[\sin\theta_1 - \sin\left(\frac{\psi_{cusp} + \theta_1}{2}\right) \right] \right\} + \tag{15}$$
$$\sqrt{\kappa_2 P R_2} \left\{ 2 \left[1 - \cos\frac{\psi_{cusp} - \theta_2}{2}) \right] \right.$$
$$+ \sin\theta_2 \left[\sin\theta_2 - \sin\left(\frac{\psi_{cusp} + \theta_2}{2}\right) \right] \right\}$$

The value of ψ_{cusp} is fixed by the boundary conditions (Eq.6)

$$\psi_{cusp} = 2\arccos\left\{ \frac{\sqrt{R_1\kappa_1}\cos\left(\frac{\theta_1}{2}\right) + \sqrt{R_2\kappa_2}\cos\left(\frac{\theta_2}{2}\right)}{\sqrt{R_1\kappa_1 + R_2\kappa_2 + 2\sqrt{R_1 R_2 \kappa_1 \kappa_2}\cos\left(\frac{\theta_1 - \theta_2}{2}\right)}} \right\} \tag{16}$$

As expected ψ_{cusp} depends on the ratio of both rigidities. However, it can not be easily measured since the size of the fold is very small compared to the vesicle size.

The parameter σ_{cusp} measures the strength of elasticity on our spherical-cap system. Note that its contribution is angular dependent. Elasticity contributes to the line tension and gives an effective line tension $\tilde{\sigma} = \sigma + \sigma_{cusp}$. However, the total line tension is now a function of all the physical constants (σ, P, κ_o and κ_d) which makes it difficult to estimate. Typical values of the elastic line tensions are $\sigma_{cusp} \simeq 10^{-14} N/m$ (see Fig. 9), for $\sigma \simeq 10^{-13} N/m$. However, the effect of σ_{cusp} on the membrane stability is given by the dimensionless number

$$n = \frac{\sigma_{cusp}}{(P\tau_c - \sigma)}$$

15

which measure the relative effect of the elastic contribution with respect to the distance at the bifurcation point. In our case, we get an important effect with $n = 38\%$ and the contribution of the elasticity to the total energy (about 4%) is not enough to affect the zero-order solution, but can be important for the fission of the vesicle.

3.2.2 Effect on the membrane shape.

The elastic terms can be taken into account by defining an effective line tension. Therefore, the previous results and the capillary solution are still valid but with a new control parameter given by $\tilde{\tau} = (\sigma + \sigma_{cusp})/P$. Note that the critical value τ_c at the bifurcation is still the same.

A variation of the control parameter $\tilde{\tau}$ modifies the angles θ_1, θ_2 and ψ_{cusp} and then the elastic line tension σ_{cusp}. The figure 7 shows the values of the reduced line tension of the fold ($\tilde{\sigma}_{cusp} = \sigma_{cusp}/P$) versus the reduced total line tension $\tilde{\tau}$. The solid line is $\tilde{\sigma}_{cusp}$ for the low energy solution. The dashed line is $\tilde{\sigma}_{cusp}$ for the high energy solution. The line tension of the fold must be smaller than the total line tension $\sigma + \sigma_{cusp}$ since the line tension σ due to the interface is positive. Therefore, some shapes are no longer physically allowed for the unstable solution. The figure 8 shows the energies of the vesicle versus the control parameter $\tilde{\tau}$ for the allowed solutions.

We have investigated the effect of the size f of the domain 1 on the elastic contribution. In the capillary model, the two domains are equivalent and τ_c is the same for f and $1 - f$. The elasticity breaks this symmetry since the two domains are no more equivalent: the l_o domain (here label 2) is harder to bend than the l_d one (here label 1). The figure 9 shows the elastic

16

line tension versus the fraction f of the domain 1. Notice that the elastic line tension is negative for large domains, meaning that the elasticity fights against pinching.

3.3 Budding by molecule insertion

The two-cap model remains a solution of the Euler-Lagrange equations when molecules are added uniformly. Eq.5 connect the concentration of molecules to the chemical potential (μ_i) and modify the area Lagrange multiplier Σ_i:

$$\mu_i = 2\frac{\Lambda_i}{R_i} - \alpha_i(\phi_i - \phi_{eq_i}) \tag{17a}$$

$$2\Sigma_i R_i^2 = PR_i^3 - 2\Lambda_i\phi_i R_i + \alpha(\phi_i^2 - \phi_{eq_i}^2)R_i^2 \tag{17b}$$

$$\gamma_i = \frac{PR_i^2}{2}\sin\psi\cos\psi \tag{17c}$$

In a previous paper, we have shown that the two-cap solutions may be unstable either above a critical homogeneous concentration given by $\bar{\phi}_{c_i} = PR_i^2/\Lambda_i$ or for very strong coupling $\Lambda_i^2/\kappa_i\alpha_i >> 1$ (Allain and Ben Amar, 2004). This instability characterizes each phase individually and not the junction between phases. Here, we focus on the junction and the experimental conditions are assumed to be below these instability thresholds.

3.3.1 Fold description

The interface is the place where strong gradients of molecule distribution are found with typical lengthscale given by

$$l_c = \sqrt{\frac{\beta_i}{\alpha_i}}$$

which must be compared to the vesicle lengthscale R_i. We focus on the case where $l_c << R_i$ so that concentration gradients are also localized at the fold

in the elastic boundary layer. For distances larger than l_c, the concentration of molecules is constant and reaches the value $\bar{\phi}_i$ that we choose as unit in each phase: so $\tilde{\phi}_i = \phi_i/\bar{\phi}$.

Far away from the fold, the sphere (denoted by S) is solution but not in the vicinity of the fold, better described by a boundary layer (denoted by B). As previously (Eq.11), we define:

$$
\begin{aligned}
\tilde{l} &= \frac{(\tilde{s} - \tilde{s}_J)}{\tilde{l}_e} \quad ; \quad \psi = \psi_S + \psi_B(\tilde{l}) \quad ; \quad r = r_S + \tilde{l}_e r_B(\tilde{l}) \quad ; \\
\gamma &= \gamma_S + \tilde{l}_e \gamma_B(\tilde{l}) \quad \text{and} \quad \tilde{\phi} = 1 + \tilde{\phi}_B.
\end{aligned}
$$

To describe the fold, we need three dimensionless parameters

$$
\tilde{l}_c = \sqrt{\frac{\beta}{\alpha R_i^2} \frac{1}{\tilde{l}_e}}, \quad \tilde{\lambda}_e = \frac{\Lambda_i \bar{\phi}_i}{P R_i^2} \frac{1}{\tilde{l}_e} \quad \text{et} \quad \tilde{\lambda}_c = \frac{\Lambda_i}{\alpha \bar{\phi}_i R_i} \frac{1}{\tilde{l}_e}. \tag{18}
$$

The conditions for the stability of both phases are $\tilde{\lambda}_e \lesssim 1$ and $\tilde{\lambda}_e \tilde{\lambda}_c \lesssim 1$. Expanding the shape equations (Eq.5) to leading order gives:

$$
\psi_B'' = \sin \psi_B + \tilde{\lambda}_e \tilde{\phi}_B', \tag{19a}
$$

$$
\tilde{l}_c^2 \tilde{\phi}_B'' = \tilde{\phi}_B - \tilde{\lambda}_c \psi_B'. \tag{19b}
$$

The fold energy in the phase i is given by the leading orders of Eq.4:

$$
\begin{aligned}
F_i &= \pi \tilde{l}_e r_J P R_i^3 \left[\int_{\mathcal{B}} \psi_B'^{\,2} d\tilde{l} - \sin \psi_S \int_{\mathcal{B}} (\sin \psi - \sin \psi_S) d\tilde{l} - 2\tilde{\lambda}_e \int_{\mathcal{B}} \psi_B' d\tilde{l} \right. \\
&\quad \left. + 4\tilde{\lambda}_e \int_{\mathcal{B}} \tilde{\phi}_B d\tilde{l} - 2\tilde{\lambda}_e \int_{\mathcal{B}} \tilde{\phi}_B \psi_B' d\tilde{l} + \frac{\tilde{\lambda}_e}{\tilde{\lambda}_c} \int_{\mathcal{B}} \tilde{\phi}_B^2 d\tilde{l} + \tilde{l}_c^2 \frac{\tilde{\lambda}_e}{\tilde{\lambda}_c} \int_{\mathcal{B}} \phi_B'^{\,2} d\tilde{l} \right]. \tag{20}
\end{aligned}
$$

The energy is the same for both phases. The sum of the two energies is proportional to r_J, the interface length, and defines a new effective line tension σ_{cusp}.

The uniform insertion of molecules in the vesicle modifies only the Lagrange multipliers which have no direct physical content, despite the modification of the energy level of the system. The two-spherical cap zeroth order solution remains valid without modification of the geometrical parameters such as radii and angles at the junction. Therefore, we conclude that the bifurcation diagram remains unchanged, except for the values of the energy, with the same threshold value found previously. For $\tau \leq \tau_c$, two ideal solutions still exist, the stable one being observed experimentally. Only gradients which appear at the interface modify the cusp shapes and we need to evaluate if they are responsible for a change in the line tension value.

The equations (19) have no explicit solution but some interesting limits can be considered. We focus here on three independent limits: $\tilde{\lambda}_e << 1$, $\tilde{\lambda}_c << 1$ and $\tilde{l}_c << \tilde{l}_e$.

First case ($\tilde{\lambda}_e << 1$): the elastic coupling length is small. This limit decouples Eq.19a at zero order, giving exactly the same solution as the case without molecule. Eq.19b allows to calculate the molecule distribution but as the terms in $\tilde{\lambda}_e$ can be neglected in the energy (Eq.20), the effect of the molecules is negligible. The elastic line tension is not modified by molecule addition.

Second case ($\tilde{\lambda}_c << 1$): the weak chemical coupling length. This limit decouples Eq.19b, leading to $\tilde{\phi}_B = \tilde{\phi}_{B_0} \exp\left(\pm \tilde{l}/\tilde{l}_c\right)$ with $\tilde{\phi}_{B_0}$ the molecule excess at the interface, given by the boundary conditions (Eq.6). In physical units and taking into account both sides of the fold, we get for the increase of the line tension:

$$\delta\sigma_{cusp} = \frac{\sqrt{\alpha_1\beta_1\alpha_2\beta_2}}{2(\sqrt{\alpha_1\beta_1} + \sqrt{\alpha_2\beta_2})}(\bar{\phi}_2 - \bar{\phi}_1)^2 \qquad (21)$$

19

The molecule absorption increases the effective line tension, which may induce the fission. This effect is only due to chemical gradients near the interface. It increases with the number of molecules added to the system.

Third case ($\tilde{l}_c << 1$): the case of a small chemical length. The molecule concentration has two very different lengthscales: l_c and l_e. The chemical length l_c contributes to the junction between the two domains and can be treated as a boundary layer. However, the associated energy is proportional to l_c and is then negligible. For size larger than l_c, Eq.19 becomes:

$$\tilde{\phi}_B = \tilde{\lambda}_c \psi'_B \tag{22a}$$

$$(1 - \tilde{\lambda}_c \tilde{\lambda}_e)\psi''_B = \sin\psi_B \tag{22b}$$

and the effective line tension in the phase i is:

$$\sigma_{cusp} = \frac{\sqrt{\kappa_i P R_i^3}}{2}\left[(1 - \tilde{\lambda}_e\tilde{\lambda}_c)\int_{\mathcal{B}}{\psi'_B}^2 d\tilde{l} - \sin\psi_S \int_{\mathcal{B}}(\sin\psi_B - \sin\psi_S)d\tilde{l}\right.$$
$$\left.+4\tilde{\lambda}_e\tilde{\lambda}_c \int_{\mathcal{B}}\psi'_B d\tilde{l} - 2\tilde{\lambda}_e \int_{\mathcal{B}}\psi'_B d\tilde{l}\right]. \tag{23}$$

Taking into account the first and second terms leads to the elastic line tension (Eq.15) with a multiplicating factor $\sqrt{1 - \tilde{\lambda}_e\tilde{\lambda}_c}$ in both phases. Note that $\tilde{\lambda}_e\tilde{\lambda}_c \geq 1$ is not possible in our framework, since the cost associated with the concentration gradients β are neglected (Allain and Ben Amar, 2004). This first contribution indicates that addition of molecules decreases the line tension associated with the elastic fold but since it does not depend on the concentration it just implies a renormalization of the bending rigidity (Leibler, 1986). The third term, proportional to $\tilde{\lambda}_e\tilde{\lambda}_c$ also decreases the line tension but does not depend on the molecules concentration. Using physical

units, the last integral contributes to the line tension by a term proportional to the concentration of added molecules:

$$\Lambda_1 \phi_1 (\theta_1 - \psi_{cusp}) + \Lambda_2 \phi_2 (\psi_{cusp} - \theta_2).$$

It is positive when the molecules are inserted in the outer monolayer of the membrane (positive Λ), which is the case found in the experiments. However, if the molecules are added in the inner monolayer, it becomes negative and budding and pinching are inhibited. In conclusion, the net effect of molecule insertion is a decrease of the line tension at low concentration, then a possibly increase as the concentration increases if the molecules are inserted from the outer monolayer.

3.3.2 Budding process

The absorption of molecules does not change the zeroth order shape equations of the stretched vesicle. It modifies the shape of the fold near the interface giving a new contribution to the effective line tension. If the absorption takes place in the external leaflet, it contributes to an increase of the line tension. This increase puts the system closer to the bifurcation point controlled by the parameter $\tilde{\tau} = (\sigma + \sigma_{cusp})/P$ and induces a budding of the smaller phase: as $\tilde{\tau}$ increases, the neck radius decreases (see Fig. 5b) and the small domain seems to lift up. If the concentration is high enough so that $\tilde{\tau} > \tau_c$, the budding is automatically followed by a fission process, creating two separated vesicles, one for each phase. If the concentration is not high enough, the lift-up will stop before the change of topology. In the meantime, it is possible that the vesicle looses some of its molecules and retracts to its initial configuration. This reversibility is impossible when fission is complete for two reasons: first,

21

the system relaxes the Gaussian elastic energy and two daughter vesicles may be energetically favored, second due to thermal fluctuations, the vesicles move away from each other and the coalescence process is unlikely. The fact that the fission occurs proves that the time scale for fission is much smaller than the possible rearrangement of molecules between the leaflets

Figure 11 reproduces experimental results from Staneva et al. (Staneva et al., 2004), showing fission of a liquid-ordered domain induced by Phospholipase A_2 proteins addition. The vesicle is obtained by electro-formation (the electrode is visible on the left of the pictures). It is composed by a 45:45:10 mol/mol mixture of phosphatidylcholine (PC), sphingomyelin (SM) and cholesterol (Chol). The vesicles includes one liquid-ordered domain visible in fluorescence microscopy (not reproduced here): a small fraction (10%) of the PC is replaced by a fluorescent lipid analog and is excluded from the l_o phase, which appears as a dark circle. The proteins are injected in the neighborhood of the vesicle by a micropipette (visible on the right of the first picture). Phospholipase A_2 activity transforms the PC lipids into LysoPC, a conical molecule, by cutting one of the two hydrophobic tails. Fission occurs about 10 seconds after protein injection.

Similar fission process have been observed when detergents like LysoPC, Triton X100 or Brij 98 are added in important quantities near a similar vesicle (Staneva et al., submitted). However, in this case, the fission is not always complete: the daughter vesicles may remain connected by a small lipid filament, as also observed in (Tanaka et al., 2004). This is not in contradiction with our model since the fission process requires to split the lipid bilayers at the molecular level, which is out of reach of our treatment. This level

requires a microscopic description as done in (Kozlovsky and Kozlov, 2003). The fission process prefers small domains, as predicted by our model. If the concentration in detergents is not high enough or if the Phospholipase A_2 is not activated, the liquid-ordered domains bud without complete fission. It is also possible to observe a relaxation of the vesicle, which recovers its initial shape.

4   Conclusion

Our model explains why ejection of a domain from an inhomogeneous vesicle can be achieved by osmotic shocks or molecule absorption. It is based on physical stability concepts in the spirit of the existence and stability analysis of the well-known catenoid. We predict a complete irreversible fission above a critical parameter. From a macroscopic point of view, the complete fission is favored, it decreases the total energy of the system at the threshold of stability because of the Gaussian energy. This fission can be inhibited if a membrane thread exists between the two phases. The existence of such a thread is out of reach of our approach. If it does not exist, the vesicles separate from each other. If it exists and if the experimental forcing relaxes, the two vesicles may fuse in principle. The experiments discussed here are in favor of a complete fission mechanism. For simplicity, the model is restricted to two domains of different sizes: extension to multi-phase domains complicates the geometry but will not change the physical results.

Acknowledgments

References

Allain, J.-M. and M. Ben Amar. 2004. Biphasic vesicle: instability induced by adsorption of proteins. *Physica A.* 337:531–545.

Allain, J.-M., C. Storm, A. Roux, M. Ben Amar and J.-F. Joanny. 2004. Fission of a multiphase membrane tube. *Phys. Rev. Lett.* 93:158104.

Baumgart, T., S. T. Hess and W. W. Webb. 2003. Imaging coexisting fluid domains in biomembrane models coupling curvature and line tension. *Nature.* 425:821–824.

Ben Amar, M., P. P. da Silva, N. Limodin, A. Langlois, M. Brazovskaia, C. Even, I. V. Chikina and P. Pieranski. 1998. Stability and vibrations of catenoid-shaped smectic films. *Euro. Phys. J. B.* 3:197–202.

Ben Amar, M. and Y. Pomeau. 1997. Crumpled paper. *P ROY SOC LOND A MAT* 453:729–755.

Bickel, T., C. Jeppesen and C. M. Marques. 2001. Local entropic effects of polymers grafted to soft interfaces. *Eur. Phys. J. E.* 4:33–43.

Brown, D. A. and E. London. 2000. Structure and function of sphingolipid- and cholesterol-rich membrane rafts. *J. Biol. Chem.* 275:17221–17224.

Chazal, N. and D. Gerlier. 2003. Virus entry, assembly, budding, and membrane rafts. *Microbiol. Mol. Biol. Rev.* 67:226–237.

de Almeida, R. F. M., A. Fedorov and M. Prieto. 2003. Sphingomyelin/phosphatidylcholine/cholesterol phase diagram: Boundaries and composition of lipid rafts. *Biophys. J.* 85:2406–2416.

Dietrich, C., L. A. Bagatolli, Z. N. Volovyk, N. L. Thompson, M. Levi, K. Jacobson and E. Gratton. 2001. Lipid rafts reconstituted in model membranes. *Biophys. J.* 80:1417–1428.

Dbereiner, H.-G., E. Evans, M. Kraus, U. Seifert and M. Wortis. 1997. Mapping vesicle shapes into the phase diagram: A comparison of experiment and theory. *Phys. Rev. E.* 55:4458–4474.

Helfrich, W. 1973. Elastic properties of lipid bilayers: Theory and possible experiments. *Z. Naturforsch A.* 33:305–315.

Holopainen, J. M., A. J. Metso, J.-P. Mattila, A. Jutila and P. K. J. Kinnunen. 2004. Evidence for the lack of a specific interaction between cholesterol and sphingomyelin. *Biophys. J.* 86:1510–1520.

Jaric, M., U. Seifert, W. Wintz and M. Wortis. 1995. Vesicular instabilities: The prolate-to-oblate transition and other shape instabilities of fluid bilayer membranes. *Phys. Rev. E.* 52:6623–6634.

Jlicher, F. and R. Lipowsky. 1996. Shape transformations of vesicles with intramembrane domains. *Phys. Rev. E.* 53:2670–2683.

Kohyama, T., D. M. Kroll and G. Gompper. 2003. Budding of crystalline domains in fluid membranes. *Phys. Rev. E.* 68:061905.

25

Kozlovsky, Y. and M. M. Kozlov. 2003. Membrane fission: Model for intermediate structures. *Biophys. J.* 85:85–96.

Laradji, M. and P. B. Sunil Kumar. 2004. Dynamics of domain growth in self-assembled fluid vesicles. *Phys. Rev. Lett.* 93:198105.

Leibler, S. 1986. Curvature instability in membranes. *J. Phys. (France).* 47:507–516.

Li, X.-M., M. M. Momsen, J. M. Smaby, H. L. Brockman and R. E. Brown. 2001. Cholesterol decreases the interfacial elasticity and detergent solubility of sphingomyelins. *Biochemistry.* 40:5954–5963.

Lipowsky, R. and R. Dimova. 2003. Domains in membranes and vesicles. *J. Phys.: Condens. Matter.* 15:S31–S45.

Lipowsky, R. and E. Sackmann. 1995. Structure and Dynamics of Membranes, Handbook of Biological Physics. Elsevier, North-Holland.

Pogorelov, A. 1988. Bending of surfaces and stability of shells. Volume 72, Translations of mathematical monographs.

Seifert, U. 1993. Curvature-induced lateral phase segregation in two-component vesicles. *Phys. Rev. Lett.* 70:1335–1338.

Seifert, U. 1997. Configurations of fluid membranes and vesicles. *Adv. in Phys.* 46:13–137.

Sens, P. 2004. Dynamics of nonequilibrium membrane bud formation. *Phys. Rev. Lett.* 93:108103.

Siegel, D. P. and M. M. Kozlov. 2004. The gaussian curvature elastic modulus of n-monomethylated dioleoylphosphatidylethanolamine: Relevance to membrane fusion and lipid phase behavior. *Biophys. J.* 87:366–374.

Simons, K. and E. Ikonen. 1997. Functional rafts in cell membranes. *nature.* 387:569–572.

Staneva, G., M. I. Angelova and K. Koumanov. 2004. Phospholipase a(2) promotes raft budding and fission from giant liposomes. *Chem. Phys. Lipids* 129:53–62.

Tanaka, T., R. Sano, Y. Yamashita and M. Yamazaki. 2004. Shape changes and vesicle fission of giant unilamellar vesicles of liquid-ordered phase membrane induced by lysophosphatidylcholine. *Langmuir.* 20:9526–9534.

van Meer, G. and H. Sprong. 2004. Membrane lipids and vesicular traffic. *Curr. Opin. Cell Biol.* 16:373–378.

Veatch, S. L. and S. L. Keller. 2003. Separation of liquid phases in giant vesicles of ternary mixtures of phospholipids and cholesterol. *Biophys. J.* 85:3074–3083.
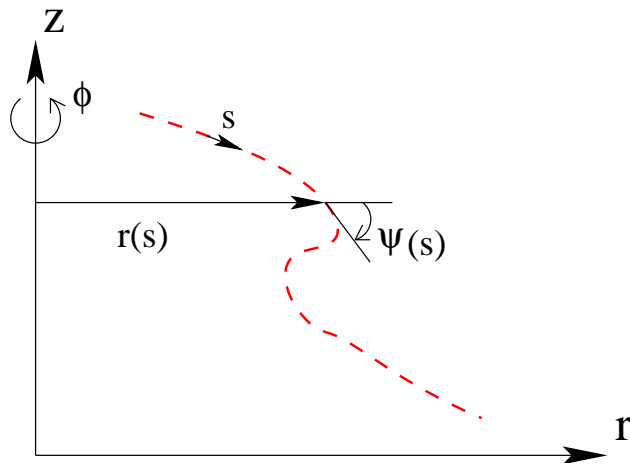
Figure 1: General parameterization of an axisymmetric vesicle in cylindrical coordinates. The dashed curve is the membrane. The parameterization is done by the arc-length s. The shape of the membrane is given by $r(s)$ and $\psi(s)$. The two domains have the same parameterization.
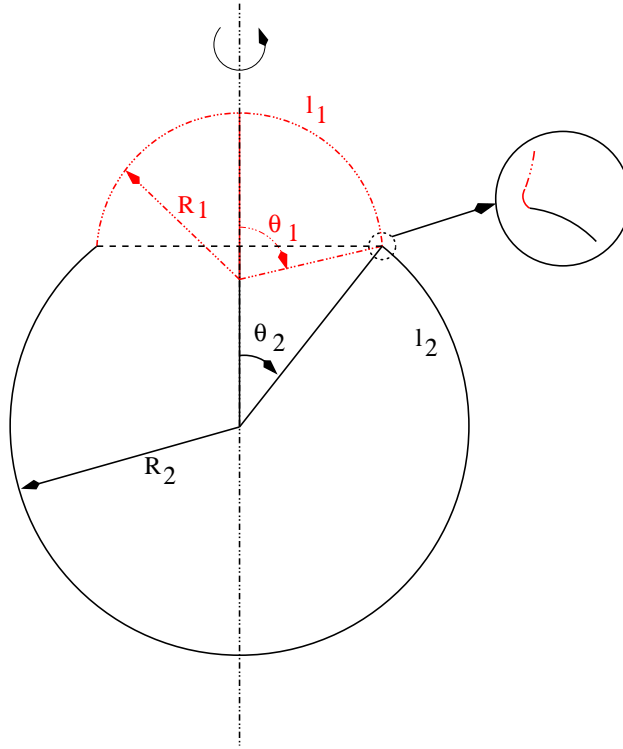
Figure 2: Schematic representation of a axisymmetric vesicle, including the four parameters R_1, R_2, θ_1 and θ_2 used in the vesicle description. The circle details the fold near the interface, where the elastic properties can no longer be neglected.

29
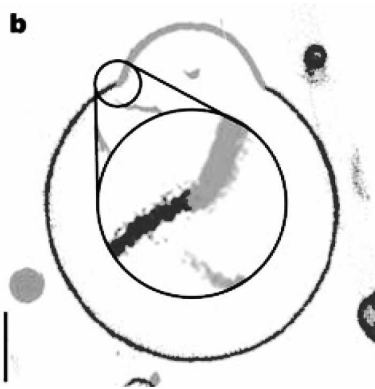
Figure 3: Black and white version of figure (1b) from Baumgart et al.'s work (Baumgart et al., 2003). The picture is a two-photon microscopy image, showing equatorial section of GUVs with two coexisting domains. The l_o domain appears in grey here and the l_d in dark. Scale bar, 5 μm. Reproduced from (Baumgart et al., 2003) with the authorizations of the authors and editor.
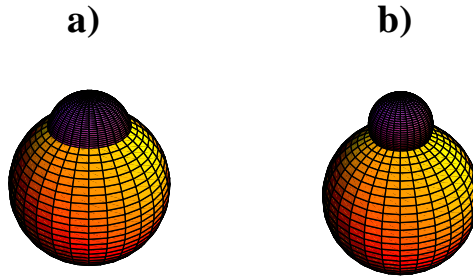
Figure 4: The two solutions of the E.-L. equations (Eq.7 and 9) for $\tau = 20.5\mu m^2$. The two pictures have the same scale. (a) Experimental solution (Baumgart et al., 2003), with $R_1 = 5.3\mu m$, $R_2 = 11\mu m$, $\theta_1 = 1.3$ and $\theta_2 = 0.51$. The associated dimensionless energy, given by Eq.10 is $\tilde{F}_{TOT} = -1.380$. (b) Calculated solution with $R_1 = 4.0\mu m$, $R_2 = 10\mu m$, $\theta_1 = 2.0$ and $\theta_2 = 0.36$. The dimensionless energy of vesicle (b) is $\tilde{F}_{TOT} = -1.377$, meaning that the solution is experimentally unstable.
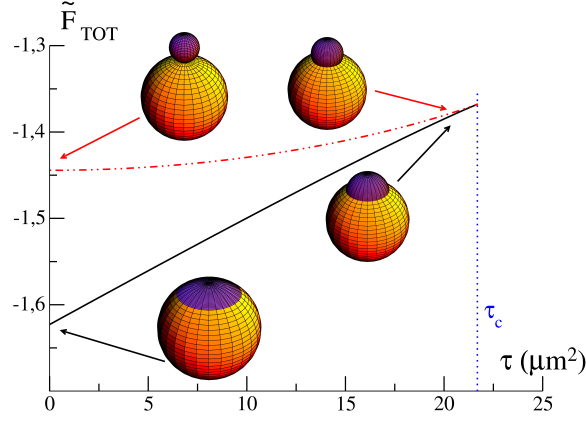
(a)
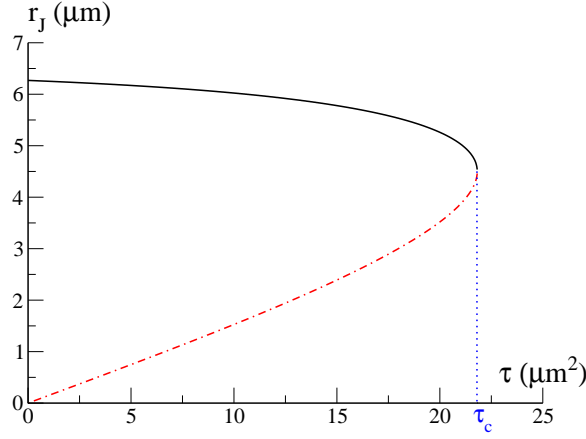
(b)

Figure 5: Dimensionless energies $\tilde{F}_{TOT}$ (figure a) and interface radius r_J (figure b) of the solutions of the E.L. equations (Eq.7 and 9) versus the control parameter $\tau = \sigma/P$. The calculation has been done with the area $A_1 = 136\mu m^2$ and $A_2 = 1296\mu m^2$. In both figures, the solid line corresponds to the stable solution, experimentally observable, the dashed line to the unstable solution and the dotted line to $\tilde{\tau} = \tilde{\tau}_c$, the critical value of the control parameter. For $\tilde{\tau} \geq \tilde{\tau}_c$, there is no longer a solution. Four pictures of vesicles showing the shape transformation with τ have been added.
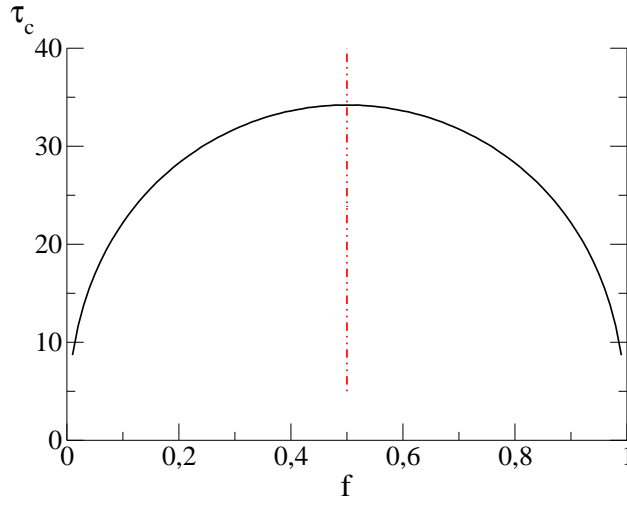
Figure 6: Values of the critical control parameter τ_c versus the fraction f of the upper domain (label 1). The calculation has been done with a fixed total area $A_{tot} = A_1 + A_2 = 1433 \mu m^2$. The areas of the domains are given by $A_1 = f A_{tot}$ and $A_2 = (1 - f)A_{tot}$. The dashed line shows the fraction 0.5.
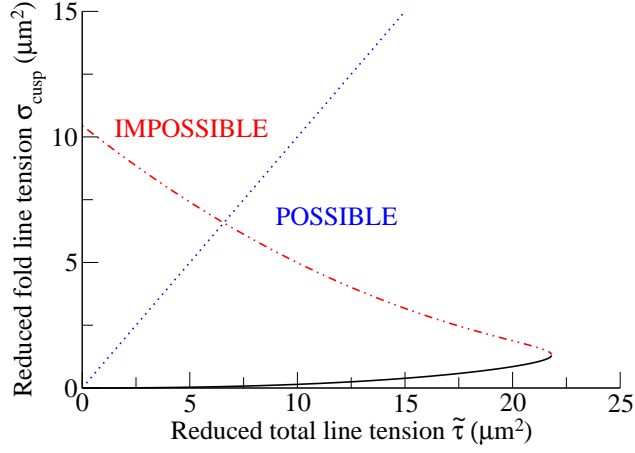
Figure 7: Reduced fold line tension σ_{cusp} versus the reduced total line tension $\tilde{\tau}$ for the two possible solutions of Eq.9. The solid line corresponds to the stable solution, the dashed line to the unstable solution. The fold line tension has been calculated using Eq.15 and 16. The parameters are $A_1 = 136\mu m^2$, $A_2 = 1296\mu m^2$ (the fixed area of each phase), $P = 10^{-2}Pa$, $\kappa_1 = 10^{-19}J$ and $\kappa_2 = 10^{-18}J$. The dotted line separates the possible solutions from the impossible one. For $\tilde{\sigma}_{cusp}$ above this line, the line tension associated to the fold is greater than the total line tension, requiring a negative line tension at the junction between the two domains, which is impossible.
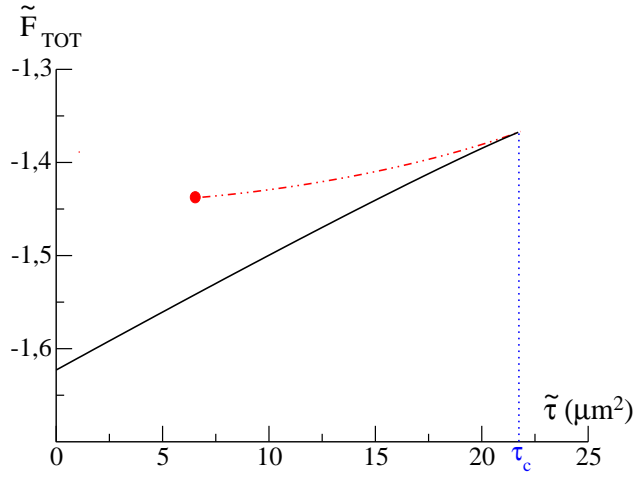
Figure 8: Dimensionless energies $\tilde{F}_{TOT}$ of the solutions of the E.L. equations (Eq.7 and 9) versus the control parameter $\tilde{\tau}$ including the effect of the elastic fold. The parameters are $A_1 = 136\mu m^2$, $A_2 = 1296\mu m^2$, $P = 10^{-2}Pa$, $\kappa_1 = 10^{-19}J$ and $\kappa_2 = 10^{-18}J$. The solid line corresponds to the stable solution,the dashed line to the unstable solution, the dotted line to $\tilde{\tau} = \tau_c$, the critical value of the control parameter. For $\tilde{\tau} \geq \tau_c$, there is no longer a solution.
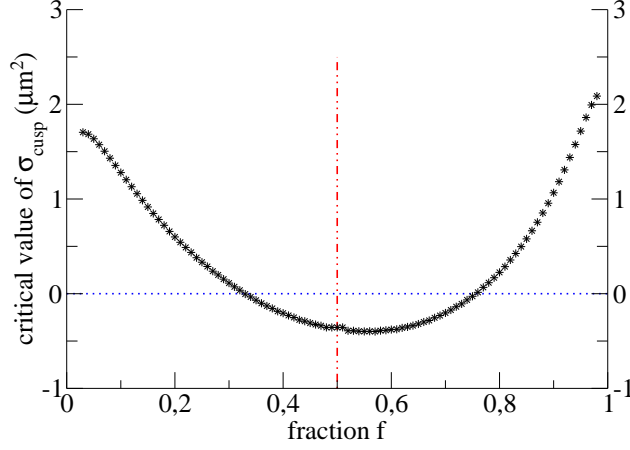
Figure 9: Fold line tension σ_{cusp} for the critical value of the total line tension $\tilde{\tau} = \tilde{\tau}_c$, versus the fraction f of the liquid-ordered domain. The calculation has been done with a fixed total area $A_{tot} = A_1 + A_2 = 1433\mu m^2$, the other parameters being $P = 10^{-2} Pa$, $\kappa_1 = 10^{-19} J$ and $\kappa_2 = 10^{-18} J$. The areas of the domains are given by $A_1 = f\, A_{tot}$ and $A_2 = (1 - f)A_{tot}$. The dashed line shows the fraction 0.5 and the dotted line $\tilde{\sigma}_{cusp} = 0$. The l_o and l_d domains (resp. label 2 and 1) do not have the same effect since the elastic moduli are not equal. Contrary to a true line tension, this effective line tension can be negative for f near 0.5.
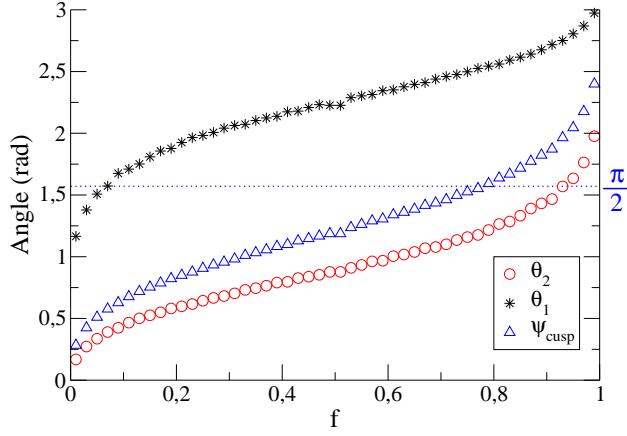
Figure 10: Angles θ_1, θ_2 and ψ_{cusp} for $\tilde{\tau} = \tilde{\tau}_c$, the critical value of the control parameter, versus the fraction f of the liquid-ordered domain. The calculation has been done with a fixed total area $A_{tot} = A_1 + A_2 = 1433\mu m^2$, the other parameters being $P = 10^{-2}Pa$, $\kappa_1 = 10^{-19}J$ and $\kappa_2 = 10^{-18}J$. Label 1 corresponds to the l_d domain and label 2 to the l_o. The areas of the domains are given by $A_1 = f A_{tot}$ and $A_2 = (1 - f)A_{tot}$. The stars are for the angle θ_1, the circles for θ_2 and the triangles for ψ_{cusp}. The angle ψ_{cusp} is always closer from the angle θ_2 since the liquid-ordered domain is hard to bend.
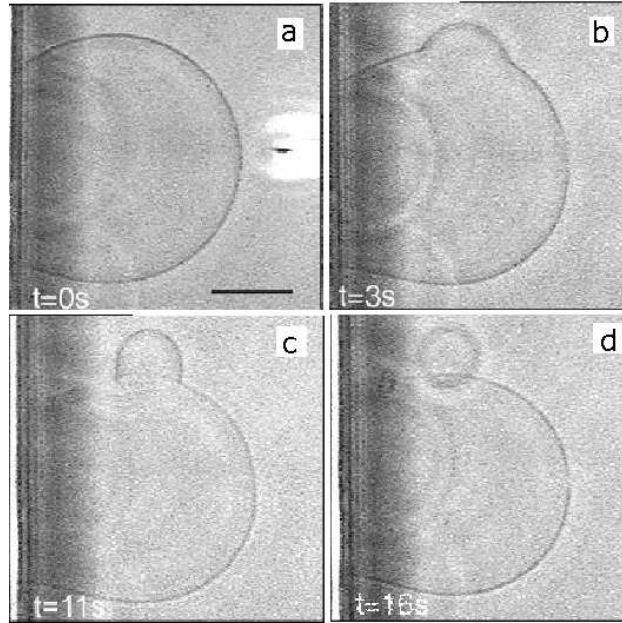
Figure 11: Ejection of a liquid-ordered domain induced by proteins Phospholipase A_2. The domain is visible on fluorescence microscopy (not reproduced here). The proteins are injected by micropipette (figure a). The liquid-ordered domain buds (figure b and c) before the fission (figure d). Reproduced form (Staneva et al., 2004) with the authorization of the editor. Bar: 20 μm.